Available online at www.sciencedirect.com
SCIENCE DIRECT®
Journal of Catalysis 225 (2004) 479–488
JOURNAL OF CATALYSIS
www.elsevier.com/locate/jcat

Nickel supported on porous silica as catalysts for the gas-phase hydrogenation of acetonitrile

A. Infantes-Molina,[a] J. Mérida-Robles,[a] P. Braos-García,[a] E. Rodríguez-Castellón,[a] E. Finocchio,[b] G. Busca,[b] P. Maireles-Torres,[a] and A. Jiménez-López [a,*]

[a] *Departamento de Química Inorgánica, Cristalografía y Mineralogía (Unidad Asociada al ICP-CSIC), Facultad de Ciencias, Universidad de Málaga, Campus de Teatinos, 29071 Málaga, Spain*

[b] *Dipartimento di Ingegneria Chimica e di Processo, Università di Genova, Ple. J.F. Kennedy, I-16129 Genova, Italy*

Received 15 December 2003; revised 30 March 2004; accepted 20 April 2004

Available online 1 June 2004

Abstract

A series of nickel supported on different porous silica catalysts (5 wt% Ni) were prepared by incipient wetness impregnation. The catalysts were characterized by XRD, H_2-TPR, N_2 adsorption at 77 K, chemisorption of H_2, and IR spectroscopy after CO and CH_3CN adsorption. Preliminary experiments have shown that the choice of nickel citrate instead of nickel nitrate as impregnation salt allows high degrees of nickel dispersion to be obtained. The catalytic behavior of this family of nickel-based catalysts reveals that the acid–basic properties of support seem to be more crucial than the extent of specific surface area and the metal particle size in determining the catalytic behavior. Thus, when nickel is supported on less acidic supports, the formation of higher amines (diethylamine and triethylamine) by condensation reactions is negligible, and full acetonitrile conversion and yields of ethylamine higher than 80 mol% at 408 K are reached.

Keywords: Hydrogenation of acetonitrile; Supported nickel catalysts; Mesoporous solids; MCM-41; Silica

1. Introduction

Lower aliphatic amines are valuable products widely used in the manufacture of medicinal, agricultural, textile, rubber, and plastic chemicals. An alternative procedure to produce amines beyond the classical liquid-phase hydrogenation reactions in the presence of metallic catalysts at high temperatures and hydrogen pressures is the gas-phase hydrogenation of nitriles [1,2].

Thus, this method seems to allow a better control of the product selectivity, since a suitable choice of the support and the active phase can lead the reaction toward a particular amine [3–7]. In this sense, Verhaak et al. [5] have observed that the use of basic supports in the preparation of nickel-based catalysts favors the formation of the primary amine. This fact led to these authors to propose a bifunctional mechanism to explain the gas-phase hydrogenation of acetonitrile, whereby the active sites for hydrogenation are located on the metal, while the acid function, which catalyzes the transamination reaction leading to secondary and tertiary amines, is situated on the support. However, this mechanistic model failed when it was applied to other catalytic systems [3,8], where all reaction steps converting nitriles into different amines seemed to take place on the surface of metal sites.

Therefore, it is evident that much work still must be done not only to tune the selectivity toward a particular amine but also to understand the mechanism implied in the gas-phase hydrogenation of nitriles.

Concerning the use of nickel-based catalysts, the incipient wetness impregnation with different salt solutions, mainly nickel nitrate, is the most extensively used method to prepare them [9–14]. However, recent works have demonstrated that nickel citrate [15–18] can give rise to catalysts with a high degree of nickel dispersion.

On the other hand, an important breakthrough in the field of porous inorganic solids was produced by researchers at the Mobil Laboratories when they reported in 1992 the development of the so-called M41S family of mesoporous solids [19,20]. Their high specific surface areas, uniform

* Corresponding author. Fax: (+34)952137534.
E-mail address: ajimenezl@uma.es (A. Jiménez-López).

0021-9517/$ – see front matter
doi:10.1016/j.jcat.2004.04.025

pore-size distributions (between 1.6 and 10 nm), and tuneable acid/base and redox properties have opened new opportunities in sorption and catalysis [21–23], as revealed by the increasing number of papers devoted to the synthesis, characterization, and applications of these solids.

Recently, we have reported that nickel supported on zirconium-doped mesoporous silica catalysts is very active in the gas-phase hydrogenation of acetonitrile at 408 K [24]. By varying the amount of nickel incorporated onto the support between 4 and 26 wt%, it was demonstrated that the turnover frequency increases with the nickel content. However, the best catalytic performance was found for a nickel catalyst prepared by ion exchange, which presented the highest nickel dispersion degree, as suggested from H_2-TPR, XRD, and H_2 chemisorption techniques. Nevertheless, the highest selectivity toward ethylamine does not exceed the value of 67 mol%, and, in all cases, the catalysts deactivate during the catalytic reaction, the conversion in the steady state ranging only between 12.2 and 30.8%.

The goal of this paper is to combine the use of different porous silica and nickel citrate as nickel impregnation salt, in order to improve the catalytic performance of supported nickel catalysts in the gas-phase hydrogenation of acetonitrile. Thus, nickel supported on several porous silica catalysts has been prepared and characterized by XRD, H_2-TPR, H_2 chemisorption, N_2 adsorption, and NH_3-TPD. We are also interested in finding out whether there is an influence of both the acidity of the support and the nickel salt used as nickel precursor on the catalytic performance.

2. Experimental

2.1. Preparation of catalysts

The mesoporous MCM-41 silica supports were prepared by adding, under vigorous stirring, tetraethoxysilane (Aldrich, 98% ethanol solution) to an aqueous solution of hexadecyltrimethylammonium bromide (25 wt%) (Aldrich), previously stirred at 353 K for 30 min. The surfactant/SiO_2 molar ratio was 0.5. The pH was adjusted to 11 by addition of an aqueous solution of tetramethylammonium hydroxide (25 wt%), and the resulting gels were stirred either at room temperature for 4 days (MCMSi) or transferred to an autoclave for hydrothermal synthesis at 398 K for 36 h (MCMSihid). In both cases, solid products were recovered by centrifugation, washed with ethanol, dried at 343 K, and then calcined at 823 K for 6 h (1 K min^{-1} heating rate).

On the other hand, a mesoporous zirconium-doped silica support (Si/Zr molar ratio = 5, denoted as MCM-SiZr) was obtained by following the procedure reported elsewhere [25]. A commercial silica (Cab-osil M-5, Fluka, $S_{BET} = 200 \pm 25$ m^2 g^{-1}) was also used as support (SiO_2). The different supports were pelletized (0.2–0.3 mm) and then impregnated by using the incipient wetness method with an aqueous solution of nickel citrate. This nickel citrate aqueous solution was prepared by mixing nickel carbonate (Aldrich) and citric acid (Sigma) in a 3:2 molar ratio in deionized water and heating until the suspension turned into a bright green solution.

Moreover, another catalyst (Ni(nit)Si) was obtained by the same impregnation procedure, but using nickel nitrate as nickel source and the mesoporous silica (MCMSi) as support. In all cases, the amount of nickel incorporated to the supports was ca. 5 wt%. After drying in air at 393 K for 12 h and calcination at 673 K for 4 h, the samples were reduced at 723 K in a H_2 flow of 50 mL min^{-1} for 60 min.

2.2. Characterization of catalysts

Powder X-ray diffraction patterns were obtained by using a Siemens D5000 diffractometer (Cu-K_α source) provided with a graphite monochromator. Textural parameters have been calculated from N_2 adsorption at 77 K carried out in a conventional glass volumetric apparatus (outgassing at 473 K and 10^{-4} mbar overnight).

Temperature-programmed desorption of ammonia (NH_3-TPD) was used to determine the total acidity of the supports. Before the adsorption of ammonia at 373 K, the samples were treated at 723 K in a helium flow (50 mL min^{-1}) for 60 min. The NH_3-TPD was performed between 373 and 1023 K, with a heating rate of 10 K min^{-1}. The evolved ammonia was analyzed by an on-line gas chromatograph (Shimadzu GC-14A) provided with a thermal conductivity detector.

The surface properties of the supported metallic nickel were obtained from hydrogen chemisorption at 298 K by using a Micromeritics ASAP 2010C apparatus. Hydrogen temperature-programmed reduction (H_2-TPR) experiments were carried out on materials previously calcined at 673 K for 4 h. The H_2 consumption was studied between 323 and 973 K, by using a flow of Ar/H_2 (48 mL min^{-1}, 10 vol% of H_2) and a heating rate of 10 K min^{-1}. Water produced in the reduction reaction was eliminated by passing the gas flow through a cold finger (193 K). The H_2 consumption was controlled by an on-line gas chromatograph (Shimadzu GC-14A) provided with a TCD.

FTIR spectra were recorded by a Nicolet Thermo Optek Nexus instrument, by using conventional IR cells connected to a gas manipulation apparatus. The catalyst pure powders were pressed into self-supporting disks and submitted to a reduction treatment consisting of heating in pure hydrogen (400 Torr) at 723 K, followed by the introduction in the IR cell itself. Before CO and acetonitrile (AN) adsorption experiments the catalysts were cooled at room temperature.

2.3. Catalytic test

The gas-phase hydrogenation of acetonitrile was performed in a flow system operating at atmospheric pressure. A tubular Pyrex reactor (27 cm length, 7 mm o.d. and 3.6 mm i.d.) was used. Prior to any measurement, 0.05 g

of sample (sieve fraction of 0.2–0.3 mm) was reduced in situ at 723 K under a hydrogen flow of 60 mL min^{-1} for 60 min (heating rate of 10 K min^{-1}). After that, the hydrogen flow was bubbled through a saturator containing acetonitrile (Aldrich, 99.93+ wt%, HPLC grade) at 283 K, thus resulting in a feed with 7.1 mol% of acetonitrile, which was introduced into the reactor. The reactants and products were analyzed by means of an on-line gas chromatograph (Shimadzu GC-14A) equipped with a flame ionization detector and a TRB-14 column. Tests were performed between 378 and 408 K, and a total flow rate of 88 mL min^{-1} was used.

The conversion is defined as

$$\text{Conversion (\%)} = 100 \times \frac{CH_3CN_{in} - CH_3CN_{out}}{CH_3CN_{in}}.$$

The selectivities were calculated from peak areas by considering the different sensitivity factors in the flame ionization detector. The selectivity for the product i is defined as

$$\text{Selectivity}_i \text{ (mol\%)} = 100 \times \frac{(\text{corrected area})_i}{\text{sum of all corrected areas}}.$$

A series of preliminary experiments were carried out in order to rule out the existence of diffusional limitations under the experimental conditions used.

3. Results and discussion

The characterization of the different mesoporous supports used in the present paper has been described and discussed elsewhere [26,27]. In all cases, the X-ray diffraction patterns of nickel supported on mesoporous silica solids exhibit, at low angles, the typical d_{100} reflection of the hexagonal arrangement of channels, indicating that the structure of the mesoporous hosts is preserved not only after conforming the powdered supports as pellets but also after the impregnation and calcination processes. However, this signal is slightly broadened due to a decrease of the long-range order. Moreover, in no cases, diffraction signals due to the presence of nickel oxide crystallites were detected at high angles in the XRD patterns of the unreduced catalysts. This is expected, taking into account the low percentage of nickel supported on the different materials, quite below the theoretical value needed for the formation of a monolayer which can be calculated from the BET surface area of the supports and the surface covered by an atom of Ni (0.065 nm^2/atom Ni).

The evaluation of the textural characteristics of the nickel oxide-based precursors and the supports has been carried out by N_2 adsorption–desorption at 77 K. These isotherms are of Type IV in the IUPAC classification and reversible, with the typical inflexion at low relative pressure (Fig. 1). The data listed in Table 1 reveal that the specific surface areas and the pore volumes were barely modified after the impregnation process, confirming that no pore blocking took place. This is due to the low loading of nickel and especially to the high dispersion degree attained by using nickel citrate as

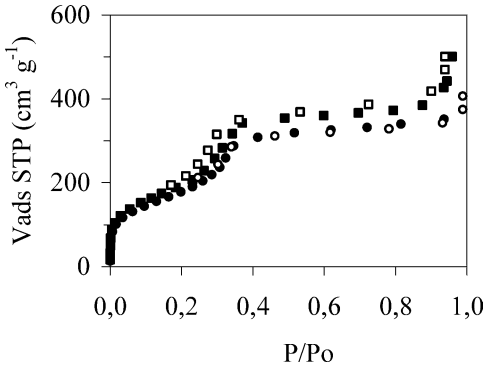

Fig. 1. N_2 adsorption–desorption isotherms at 77 K for MCMSihid support (■, adsorption; □, desorption) and unreduced NiSihid catalyst (●, adsorption; ○, desorption).

Table 1
Textural characteristics of the supports and the nickel-based catalysts

Support	S_{BET} (m^2 g^{-1})	V_P (cm^3 g^{-1})	Catalyst	S_{BET} (m^2 g^{-1})	V_P (cm^3 g^{-1})
MCMSi	749	0.567	NiSi	665	0.439
			Ni(nit)Si	577	0.479
MCMSihid	700	0.606	NiSihid	674	0.559
SiO_2	179	0.509	$NiSiO_2$	173	0.523
MCMSiZr	444	0.342	NiSiZr	434	0.301

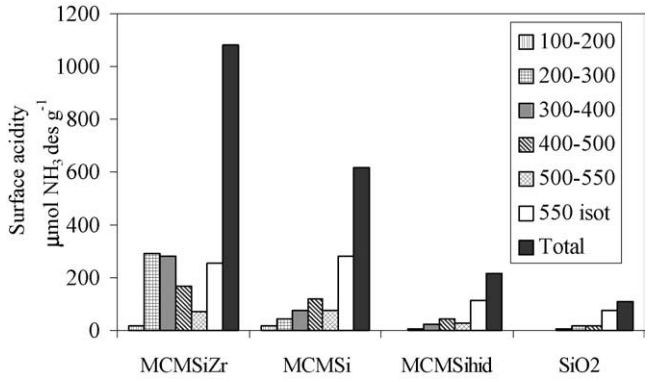

Fig. 2. Acidity of the different supports as determined by NH_3-TPD.

precursor salt. However, a most important reduction of both textural parameters is observed when nickel nitrate is used as precursor salt, Ni(nit)Si, pointing to the presence of larger metal oxide particles, perhaps partially blocking a fraction of pores.

On the other hand, it has been previously reported that the selectivity in the gas-phase hydrogenation of acetonitrile depends on the acidity of the support [5,28,29]. For this reason the acidity of the different supports used in this study was evaluated by NH_3-TPD. This technique confirms the results previously obtained with other members of the MCM-41 family, which have demonstrated that the incorporation of heteroatoms such as aluminum or zirconium enhances the acidity of the inorganic framework. Thus, the acidity increases from 614 for MCMSi to 1081 μmol NH_3 g^{-1} after the incorporation of zirconium into the mesoporous silica,

MCMSiZr (Fig. 2). By comparing the different porous silica, the acidity decreases in the order MCMSi > MCMSihid > SiO_2. This evolution is expected taking into account that, in the case of MCM-41-based solids, the hydrothermal treatment leads to a more ordered mesoporous solid, with a low content of structural defects and a higher degree of condensation of silanol groups, and hence to the low acidity observed. In the case of SiO_2, it possesses a low surface area and the presence of silanol groups is scarce.

Concerning the H_2-TPR study of supported nickel catalysts, it is well documented since numerous papers have dealt with this technique, the important influence of parameters such as the calcination temperature of impregnated samples, the nature of the nickel precursor and the support, the nickel loading, and the incorporation method (impregnation, ion exchange, deposition–reduction) on the H_2-TPR profiles. In our case, the hydrogen consumption can only be attributed to the reduction of Ni(II), since after calcination of the catalyst precursors at 673 K, neither citrate nor nitrate residues were detected by CHN analysis. The supported MCMSi catalyst prepared by using nickel nitrate, Ni(nit)Si, presents a H_2-TPR profile quite different from those of the catalysts obtained using nickel citrate as impregnation salt (Fig. 3). Thus, a main peak at 629 K together with a shoulder at 604 K and a broad band centered at 700 K are observed for Ni(nit)Si, whereas the other catalysts exhibit a very broad signal of H_2 consumption with the maximum between 720 and 820 K, and a small peak at 565–600 K. The peaks observed at low temperatures coincide approximately with that corresponding to bulk NiO (613 K), indicating the presence of a variable fraction of large nickel oxide particles. These NiO particles must be rather larger than those associated with the reduction bands appearing at higher temperatures. These H_2-TPR results are in agreement with those reported by Lensveld et al. [17], which have demonstrated that nickel oxide can be well dispersed on mesoporous materials by using incipient wetness impregnation with an aqueous solution of nickel citrate. This specific behavior confirms the existence of nickel(II) species strongly interacting with the support, and also being difficult to reduce, avoiding the sintering of the metal particles during the reduction process. This has been explained as a consequence of the formation of chelated nickel species from nickel citrate, which are arranged as a wetting and highly viscous film on the surface of the support, which upon calcination is broken up and decomposed resulting in the formation of very small nickel oxide particles. On the other hand, the maximum reduction peak for NiSi appears at higher temperatures than those corresponding to NiSihid, indicating as expected the existence of a stronger nickel oxide–support interaction for the NiSi material due to the more disordered structure of the support prepared at room temperature, in agreement with the acidity data previously discussed.

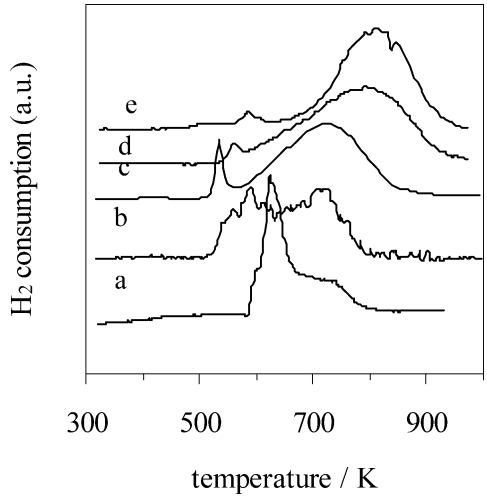

Fig. 3. H_2-TPR curves for: (a) Ni(nit)Si, (b) $NiSiO_2$, (c) NiSihid, (d) NiSi, and (e) NiSiZr.

The H_2-TPR curve of $NiSiO_2$ is also quite different, showing two maxima of reduction at 600 and 725 K, revealing the presence of two types of NiO species interacting differently with the support. The first peak could correspond to large particles while the second one would indicate the existence of well-dispersed nickel oxides on this support.

We have previously pointed out that the reducibility of nickel species also depends on the nature of the support [30] and, in general, a strong metal–support interaction (SMSI) is found for more acidic supports. This is the case for NiSiZr, which exhibits a H_2-TPR profile similar to that of samples prepared from nickel citrate on mesoporous silica, but the reduction peaks shifted at higher temperatures, as expected by considering the stronger interaction between the nickel oxide and this more acidic support. Furthermore, the H_2-TPR curve of NiSiZr differs from those observed for analogous catalysts prepared by using nickel nitrate as nickel source, in which the main hydrogen consumption was detected at lower temperatures, pointing out the presence of large nickel oxide particles [24].

The degree of nickel dispersion was evaluated from the H_2 chemisorption data by assuming that the ratio of the total amount of adsorbed hydrogen atoms to exposed Ni atoms is 1:1 (Table 2). After reduction at 723 K, the reduction percentages, as determined from the H_2-TPR curves, range between 46 and 100%. The Ni(nit)Si shows the maximum degree of reduction but poor dispersion, similar to that of nickel supported on a commercial silica, $NiSiO_2$. The two

Table 2
Nickel content and metallic characteristics of the supported nickel catalysts

Catalyst	α (%)	D (%)	Metallic surface		d (nm)
			$m^2\ g_{cat}^{-1}$	$m^2\ g_{M^\circ}^{-1}$	
NiSiZr	46	5.11	0.8	33.2	7.5
NiSi	64	7.33	1.5	47.6	7.3
Ni(nit)Si	100	3.30	1.1	21.4	25.3
NiSihid	74	10.35	2.5	67.2	6.0
$NiSiO_2$	100	2.80	0.9	18.2	29.9

α is the reduction degree determined by H_2-TPR, D the metallic dispersion, and d the average diameter of the metallic crystallite.

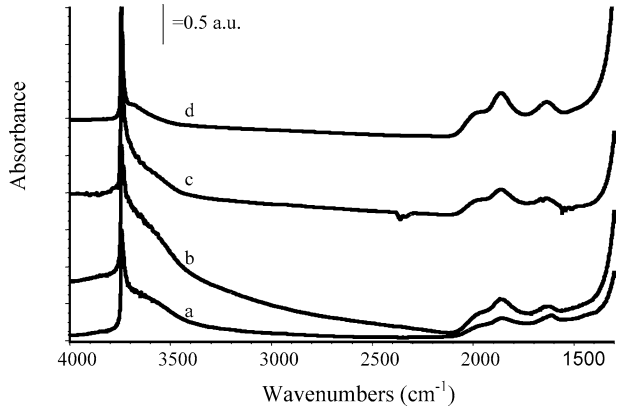

Fig. 4. FTIR spectra of (a) MCMSiZr, (b) reduced NiSiZr, (c) reduced NiSi, and (d) reduced $NiSiO_2$, after outgassing at 673 K.

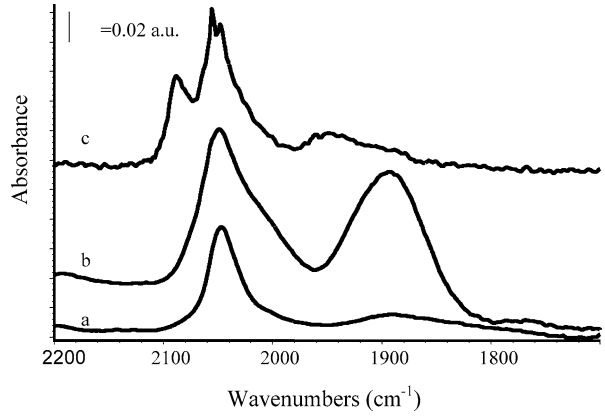

Fig. 5. FTIR spectra at room temperature arising from CO adsorption over (a) reduced NiSi, (b) reduced $NiSiO_2$, and (c) NiSiZr. (Gas phase CO spectrum has been subtracted.)

catalysts prepared by using mesoporous silica as support, NiSi and NiSihid with the highest surface area, exhibit better dispersion and the highest metallic surface.

The adsorption of probe molecules such as CO and CH_3CN and their study by FTIR spectroscopy is thoroughly applied to investigate the surface characteristics of supported catalysts. The spectra of the reduced Ni-containing catalysts after the respective activation procedures and the MCMSiZr support (Fig. 4) show the absorption cutoff near 1250 cm^{-1} due to the bulk absorption of the silica-based framework, and the typical overtone spectrum with maxima at 1610 and 1860 cm^{-1} and an evident shoulder centered near 1950 cm^{-1}. At higher frequencies, the very sharp peak due to the OH stretching of the free surface hydroxyl groups and a broad feature associated to H-bonded OHs are evident. The spectra are closely similar, although the intensity of the band of terminal silanols is decreased in intensity in the sample with 5 wt% Ni, with respect to the MCMSiZr support, possibly due to the partial ion exchange of the OHs.

The spectra of CO adsorbed at room temperature on the Ni-containing catalysts (NiSiZr, NiSi and $NiSiO_2$), after reduction at 723 K, are reported in Fig. 5 (the gas-phase absorptions are subtracted). Under these conditions, the main band of the spectrum is centered around 2050 cm^{-1} in all the spectra and is assigned to the CO stretching of terminal carbonyls on reduced Ni metal centers. This band is typical for CO linearly adsorbed on Ni particles on silica [31].

In the spectrum of NiSiZr sample an additional sharp component at 2090 cm^{-1} can be due to CO linearly bonded on smaller Ni particles, whose electron density is reduced by interaction with Zr cations. A strong metal–support interaction has also been proposed to explain the H_2-TPR profile for this sample. In the spectrum of CO over $NiSiO_2$ (Fig. 5,b), a broad and strong band is also detected around 1890 cm^{-1} due to bridging (actually threefold bridging) CO over metal centers. The presence of this band can be taken as an indication of the presence of large metal particles. In the other spectra we detected only a very weak absorption in this range. These data confirm the H_2-TPR results, pointing out the formation of larger particles after Ni reduction in the

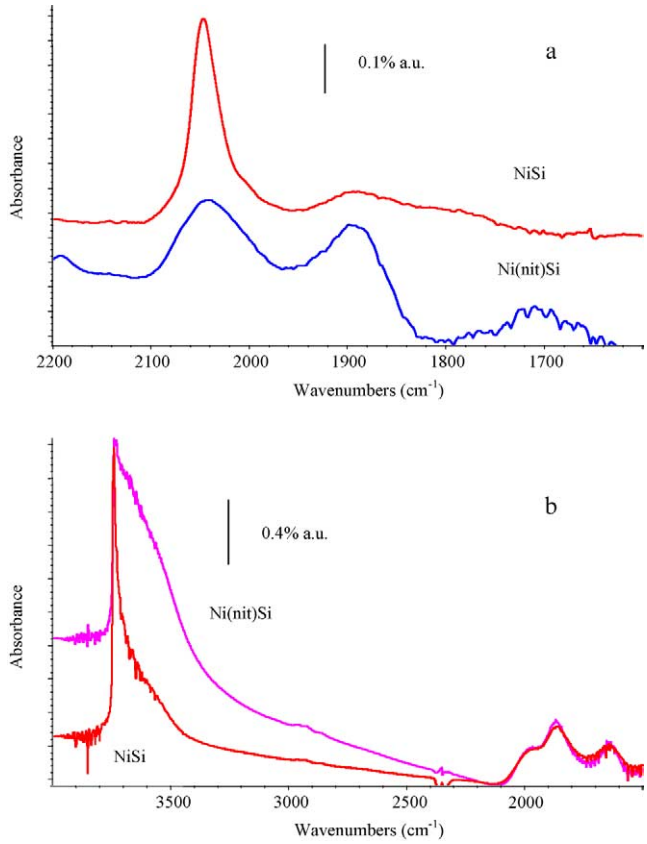

Fig. 6. (a) FTIR spectra at room temperature arising from CO adsorption over reduced NiSi and Ni(nit)Si samples, (b) FTIR spectra in the OH region of reduced NiSi and Ni(nit)Si, after outgassing at 673 K.

$NiSiO_2$ sample, probably together with well-dispersed particles.

The FTIR spectra, after CO adsorption over Ni(nit)Si and NiSi catalysts, reveal the existence of two IR bands at 2040 and 1898 cm^{-1}, characteristics of CO bonded to Ni metal centers (Fig. 6a). However, the second band (assigned to threefold bridging CO) is far less intense in the spectrum of NiSi. Differently, the presence of this band at lower fre-

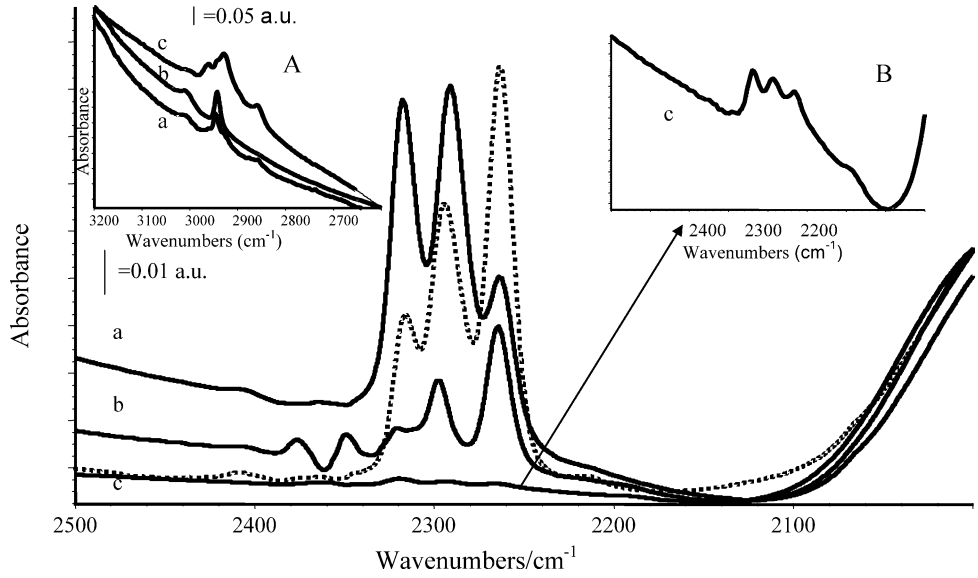

Fig. 7. FTIR spectra after CH_3CN adsorption and following outgassing at room temperature over (a) reduced NiSiZr, (b) reduced NiSi, (c) reduced $NiSiO_2$, and MCMSiZr support (dashed line). (Inset A) CH-stretching region. (Inset B) Spectrum c, enlargement in the CN-stretching region.

quency points out the existence of larger metal particles on the surface of the catalyst prepared by using nickel nitrate as nickel source, Ni(nit)Si, and agrees well with the H_2-TPR data. Moreover, this less dispersed catalyst leaves a higher fraction of acid sites available on the surface, as revealed the IR spectrum in the OH region, where a broad band due to silanol groups is observed (Fig. 6b).

As regards the IR spectrum of pure acetonitrile, in the CN-stretching region, it presents a doublet due to the Fermi resonance between the CN-stretching fundamental and the $\delta CH_3/\nu CC$ overtone modes, with the lower frequency band more intense than the higher frequency band. In Fig. 7 the spectra of the support MCMSiZr and of the catalysts (NiSiZr, NiSi and $NiSiO_2$) are shown after contact with acetonitrile and following outgassing at room temperature. Three bands are observed in each spectrum, centered almost at the same wavenumbers, around 2315, 2295, and 2260 cm^{-1}. However, their behavior in dynamic vacuum is quite different. In the MCMSiZr spectrum (dashed line) the three bands decrease in parallel by outgassing, so that after half-an-hour outgassing, the lower frequency band is still the most intense, but all decreased significantly. On the contrary, on the NiSiZr catalyst (Fig. 7a) the band at 2260 cm^{-1} is the most intense in the spectrum recorded in contact with the gas, but, after outgassing, it almost disappeared. Under these conditions also the band in the middle, observed at 2293 cm^{-1}, strongly decreased in intensity while that at the highest frequencies, i.e., at 2316 cm^{-1}, is almost unaffected. As confirmed by subtraction spectra, outgassing causes the desorption of the species responsible for the doublet at 2263 and 2296 cm^{-1} (Fermi resonance doublet of weakly adsorbed acetonitrile). The position of these two components is only slightly shifted upward with respect to liquid acetonitrile while also the relative intensity is not changed very much. The doublet for the more resistant species is at 2318 and 2291 cm^{-1}, their relative intensity being very similar, and is typically found for acetonitrile interacting with medium-strong Lewis acid sites [32].

The spectrum of acetonitrile adsorbed on the MCMSiZr support (dashed line) can be interpreted in parallel with those of pivalonitrile adsorbed on the same material [26]. The doublet at higher frequencies (2316 and 2293 cm^{-1}) is assigned to acetonitrile interacting with Lewis acidic sites associated to Zr^{IV} deficiently coordinated, while the doublet at 2295 and 2265 cm^{-1} is due to acetonitrile H-bonded over silanol groups. The slight but evident increase in intensity of the higher frequency doublet in the NiSiZr spectrum with respect to that of the support and the definite stronger stability suggest that in this case this doublet is mainly due to acetonitrile adsorbed on Ni particles, acting as medium-strong Lewis sites, although the contribution of acetonitrile adsorbed on Ni^{2+} acid sites could not be discarded, considering the low reduction percentage of NiSiZr, deduced by H_2-TPR (46%).

In the case of Ni supported over MCMSi and SiO_2 (Fig. 7, spectra b and c, enlarged in the inset) acetonitrile adsorption reveals Lewis-bonded acetonitrile, absorbing at 2318 and 2293 cm^{-1}, which must be due to the molecule bonded to Ni particles. In fact the spectra of nitrile coordinated over pure SiO_2 and MCMSi supports show only the features due to acetonitrile interacting with OH groups [33]. However, the spectrum of acetonitrile on $NiSiO_2$ in the CN-stretching region shows peaks which are by far less intense than in the previous cases (NiSiZr and NiSi samples), and the IR features in the CH-stretching region are also quite different, in comparison with νCH of molecularly adsorbed AN (Fig. 7). Possibly some reduction occurred with hydrogen still present in the metal, even after outgassing. From these data, we can infer a different behavior for $NiSiO_2$ and NiSi catalysts with respect to that of NiSiZr. In the latter,

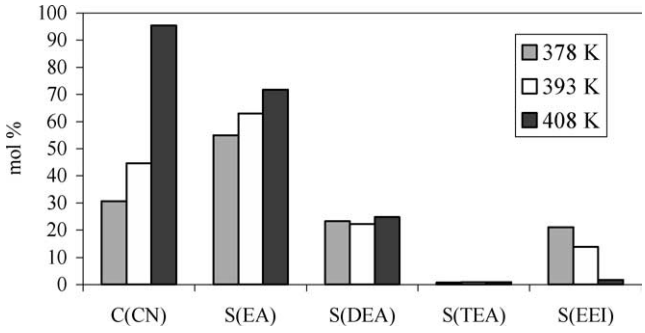

Fig. 8. Evolution of conversion and selectivity with the temperature for NiSi catalyst.

acetonitrile molecules mainly interact with the metallic particles, whereas in the silica-based catalysts the interaction by hydrogen bonding with the silanol groups appears to be more important. The strong metal–support interaction between the small nickel particles and the MCMSiZr support makes them electron deficient and thereby their acidity is increased and in consequence the affinity toward the basic acetonitrile molecules is higher.

This family of nickel-based catalysts has been tested in the gas-phase hydrogenation of acetonitrile. The reaction products were ethylamine (EA), diethylamine (DEA), triethylamine (TEA), *N*-ethylethylimine (EEI), and traces of methane.

The study of the influence of the reaction temperature on the acetonitrile hydrogenation has been carried out by using the NiSi catalyst (Fig. 8). The corresponding data in the steady state (after 15 h of time on stream, TOS) reveal that by increasing the temperature from 378 to 408 K an important amelioration of the catalyst performance is produced, raising the conversion from 31 to 95%. Concerning the selectivity toward the different products, the production of EA increases from 55 to 72 mol%, whereas the selectivities toward DEA and TEA are barely modified. *N*-ethylethylimine was only observed at low temperatures and conversion, as previously reported by Medina et al. [6]. It is supposed that by increasing the temperature the desorption of EA from the hydrogenation sites is favored, and its transformation into the EEI intermediate, precursor of the higher amines, is minimized. Therefore, it is evident that the catalytic activity is excellent at 408 K, with high CH_3CN conversion and selectivity to EA. In consequence, this temperature was selected for all ulterior catalytic studies.

The influence of the nickel source used in the preparation of supported nickel catalysts has also been evaluated. For this, two nickel catalysts were prepared by supporting nickel nitrate and nickel citrate on the mesoporous MCMSi. In both cases, the initial acetonitrile conversion values, calculated by extrapolating to zero time, are 100% (Fig. 9). However, their catalytic behavior in the steady state (Table 3) is very different since the conversion and the turnover frequency for NiSi are much better than that of Ni(nit)Si. This could be explained by taking into account the greater dispersion and metallic surface area of the NiSi catalyst (Table 2). Moreover, by considering the selectivity, both catalysts also show very distinctive patterns. Thus, whereas NiSi exhibits a high selectivity to EA, Ni(nit)Si favors the formation of the intermediate EEI. However, these differences cannot be easily explained from the point of view of the metallic properties, but perhaps the different nature of the species present on the catalyst surface might be considered. If we consider the acid–base interaction between the support and the different molecules present in the reaction media, whose basic character follows the order $CH_3CN < EA < TEA < DBA$ [34], the selectivity to condensation products might be influenced by the acidity.

In fact, Ni(nit)Si is drastically deactivated whereas NiSi maintains its conversion practically constant after 18 h of TOS. The metallic particles of the NiSi catalyst, prepared from nickel citrate, seem to cover the majority of strong acid centers, in such a way that dehydrogenation of acetonitrile does not take place, and avoiding the catalyst deactivation by the presence of partially dehydrogenated acetonitrile species, as previously reported by Verhaak et al. [35]. In contrast, the Ni(nit)Si catalyst with a poor metallic dispersion leaves a high fraction of acid sites accessible to acetonitrile molecules, where they give rise to carbonaceous products. In consequence, the more acidic Ni(nit)Si catalyst can retain more strongly EA and favors the formation of EEI, a more condensed molecule. The results obtained with NiSihid and especially with $NiSiO_2$ corroborate this assumption, because both are less acidic supports (Fig. 2), and they give rise to a low proportion of condensed products and a high formation of EA (Table 3). Finally, the NiSiZr catalyst, prepared with the more acidic MCMSiZr support and nickel citrate, exhibits a low conversion in the steady state and the formation of DEA and EEI is considerable. However, the conversion of this catalyst is higher than that of a similar catalyst prepared from nickel nitrate [24].

In the hydrogenation of CH_3CN over NiSiZr catalysts, prepared from nickel nitrate, we have previously reported that all catalysts are drastically deactivated during the catalytic run, and the extent of deactivation seems to depend on both the nickel loading and the nickel incorporation method [24]. Huang et al. [7] have found that in the gas-phase hydrogenation of acetonitrile over Ru/NaY at 160 °C and over Pt/NaY at 110 °C, metal agglomeration is the major cause of catalyst deactivation, and this loss of activity outweighs any beneficial effect of the higher TOF on large metal particles if present, as previously reported by other authors by considering a structure-sensitive reaction [8,36]. In our case, we have found that the deactivation is more important when the production of the tertiary amine is high at the beginning of the catalytic reaction. Thus, the Ni(nit)Si and NiSiZr catalysts exhibit initial selectivities toward TEA of 17.2 and 24.4 mol%, respectively, whereas for NiSihid it is only 3.6 mol%. From the IR studies of CH_3CN adsorbed on our nickel-based catalysts, we have observed that the interaction of acetonitrile with metallic nickel is very weak when

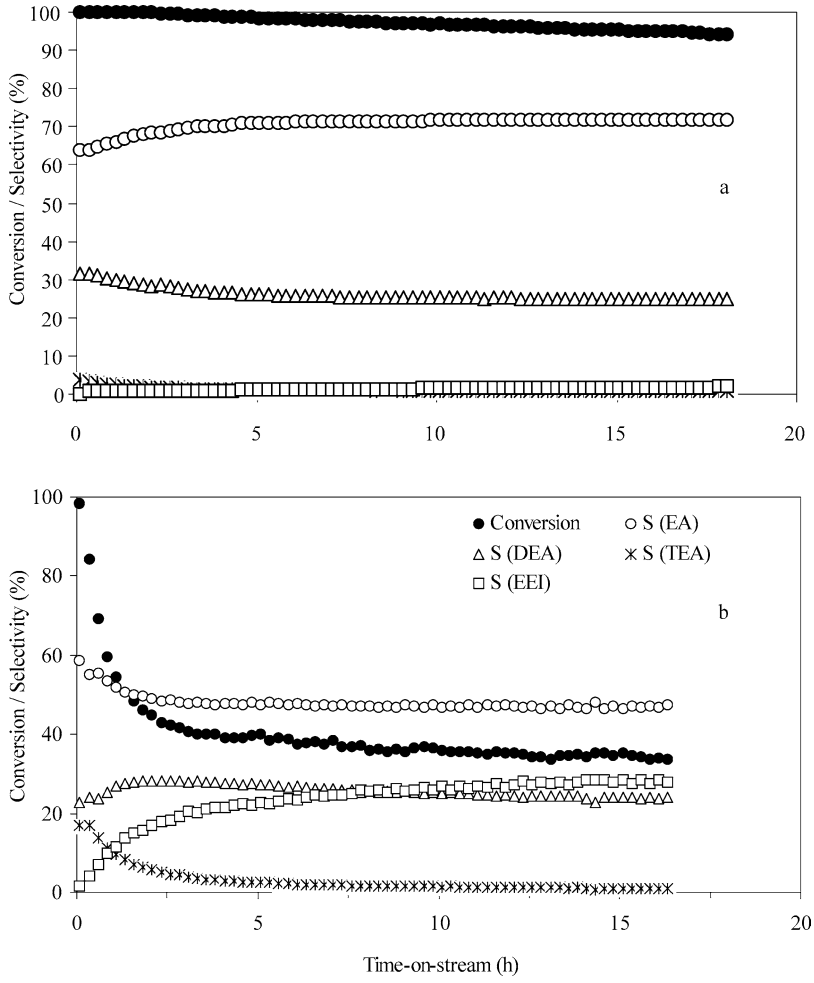

Fig. 9. Variation of conversion and selectivity as a function of time on stream on (a) NiSi and (b) Ni(nit)Si catalysts.

Table 3
Catalytic properties of the supported nickel catalysts in the hydrogenation of acetonitrile at 408 K in the steady state (H_2/CH_3CN molar ratio = 15)

Catalyst	Turnover frequency (molec CH_3CN conv at_{Ni}^{-1} s^{-1})	Conversion (%)	Product selectivity (mol%)			
			EA	DEA	TEA	EEI
NiSiZr	0.032	45	42.3	32.5	4.3	20.9
NiSi	0.068	95	71.8	24.9	0.9	1.7
Ni(nit)Si	0.025	35	46.6	24.0	1.1	28.3
NiSihid	0.066	100	73.5	23.7	1.3	0.6
$NiSiO_2$	0.069	100	86.8	12.2	0.5	0

Table 4
Chemical analyses of spent catalysts

Catalyst	Chemical analysis (wt%)		
	C	N	C/N
NiSiZr	2.98	0.91	3.27
NiSi	3.74	0.86	4.34
Ni(nit)Si	4.73	1.06	4.46
NiSihid	3.78	1.09	3.47
$NiSiO_2$	1.74	0.55	3.17

supported on a commercial silica ($NiSiO_2$). Perhaps this fact is responsible of the absence of deactivation of this catalyst, since active sites are easily available to new molecules to be hydrogenated. On the contrary, the NiSiZr catalyst with the greatest interaction between the acetonitrile molecules and the metallic particles, as deduced from the IR study of adsorbed acetonitrile, suffers maximum deactivation, possibly due to the retention on metal particles of TEA and DEA. In fact, the C/N weight ratios (Table 4) found over the spent catalysts (3.2–4.5) point to the presence of higher amines on the catalyst surface. The presence of TEA on the active sites has been postulated as responsible for the deactivation of nickel-based catalysts in the gas-phase hydrogenation of acetonitrile [37]. In any case, the catalytic activity of deactivated catalysts can be easily recovered by treatment at 673 K for 1 h in a flow of H_2.

Over prereduced NiSiZr, we have also performed acetonitrile hydrogenation experiments in the IR cell (Fig. 10). At room temperature we detected features due to molecularly adsorbed acetonitrile: bands at 3005 and 2943 cm^{-1} (CH_3-stretching modes) and 1444, 1417, and 1374 cm^{-1}, sharp, CH deformation modes, together with bands in the CN-stretching region, discussed before. These species are

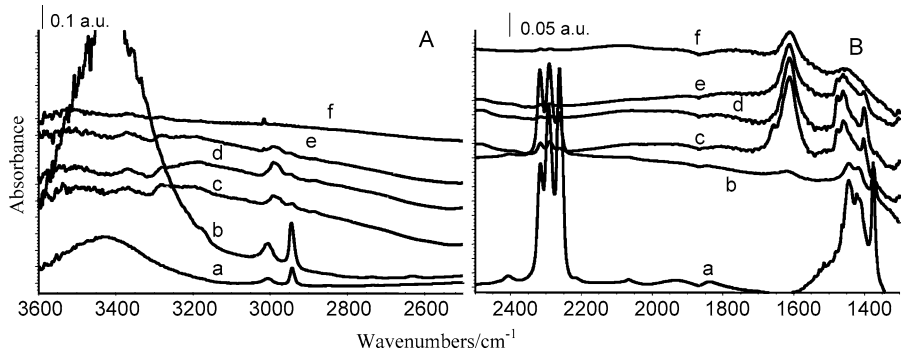

Fig. 10. FTIR spectra arising from CH_3CN adsorption over reduced NiSiZr (a) at room temperature, (b) after outgassing at room temperature for 30 min, (c) after heating in the presence of H_2 at 373 K, (d) at 473 K, (e) at 523 K, (f) at 573 K. (A) CH and NH-stretching region. (B) CN-stretching and CH deformation region.

resistant to outgassing at room temperature. Heating the catalyst surface at 373 K in the presence of hydrogen gives rise to adsorbed products characterized by bands at 2993, 2943 (very weak), and 2890 cm^{-1}, weak, due to CH stretching, and by bands at 1476, 1459, and 1401 cm^{-1}, due to CH deformations. New bands at 1656 cm^{-1}, shoulder, and at 1611 cm^{-1} are also detected, together with features in the NH-stretching region around 3365, 3282, and 3188 cm^{-1}, broad and complex. Bands due to adsorbed acetonitrile have almost completely disappeared. This is a quite complex pattern, clearly showing the presence of adsorbed reaction products. The overall spectrum suggests the presence of aliphatic amines, in particular the strong band around 1611 cm^{-1} can be assigned to the NH_2 deformation mode, thus pointing out the presence of primary (likely ethyl-)amine [38]. The shoulder at 1656 cm^{-1} can be assigned to the C=N-stretching mode of ethylideneimine [39]. The imine seems to be stable at the surface only below 473 K. At the highest temperatures (523–573 K), CH_4 is also detected (νCH band at 3016 cm^{-1}).

4. Conclusions

By comparing the catalyst prepared on zirconium-doped mesoporous silica with those reported in Ref. [24], it can be inferred that the use of nickel citrate clearly ameliorates the catalytic performance, as revealed from the higher conversion in the steady state (45%), thus reaching a TOF value of 0.032 molec CH_3CN converted at$_{Ni}^{-1}$ s^{-1}. However, the selectivity toward EA only increases up to 42.3 mol%. This fact has been corroborated by studying two nickel supported on mesoporous silica catalysts, prepared from nickel nitrate and nickel citrate. Thus, the use of nickel citrate has allowed us to prepare supported silica catalysts which give rise to a full acetonitrile conversion and EA selectivity higher than 80 mol%.

The present study also provides evidence of the influence of the support acidity on both the acetonitrile conversion and the selectivity toward the different amines on nickel-based catalysts, thus confirming previous data reported by other authors [6]. The catalytic behavior of this family of catalysts reveals that the acid–basic properties of support seem to be more crucial than the specific surface area and the metal particle sizes in determining the catalytic behavior. Thus, when nickel is supported on less acidic supports (NiSihid and $NiSiO_2$), the contribution of the condensation reactions leading to higher amines (DEA, TEA) to the selectivity patterns is negligible, and high yields of EA are reached.

Acknowledgments

We gratefully acknowledge the Ministerio de Ciencia y Tecnología (Spain) for funding this work under Project MAT2003-02986. A.I.M. also thanks the Ministerio de Ciencia y Tecnología (Spain) for a fellowship.

References

[1] K. Weissermel, H.J. Arpe, Industrial Organic Chemistry, Chemie, Berlin, 1978.
[2] M. Grayson (Ed.), Kirk–Othmer Encyclopedia of Chemical Technology, vol. 2, second ed., Wiley Intersciences, New York, 1983.
[3] Y. Huang, W.M.H. Sachtler, Appl. Catal. A 182 (1999) 365.
[4] C.V. Rode, M. Arai, M. Shirai, Y. Nishiyama, Appl. Catal. A 148 (1997) 405.
[5] M.J.F.M. Verhaak, A.J. van Dillen, J.V. Geus, Catal. Lett. 26 (1994) 37.
[6] F. Medina, R. Dutartre, D. Tichit, B. Coq, N.T. Dung, P. Salagre, J.E. Sueiras, J. Mol. Catal. A 119 (1997) 201.
[7] Y. Huang, V. Adeeva, W.M.H. Sachtler, Appl. Catal. A 196 (2000) 73.
[8] M. Arai, Y. Takada, Y. Nishiyama, J. Phys. Chem. B 102 (1998) 1968.
[9] A. Corma, A. Martínez, V. Martínez-Soria, J.B. Montón, J. Catal. 153 (1995) 25.
[10] T. Halachev, R. Nava, L. Dimitrov, Appl. Catal. A 169 (1998) 111.
[11] J. Cui, Y.H. Yue, Y. Sun, W.Y. Dong, Z. Gao, Stud. Surf. Sci. Catal. 105 (1997) 687.
[12] Y. Yue, Y. Sun, Z. Gao, Catal. Lett. 47 (1997) 167.
[13] M. Hartmann, A. Pöppl, L. Kevan, J. Phys. Chem. 100 (1996) 9906.
[14] T. Klimova, J. Ramírez, M. Calderón, J.M. Domínguez, Stud. Surf. Sci. Catal. 117 (1998) 493.
[15] G.R. Meima, B.G. Dekker, A.J. van Dillen, J.W. Geus, J.E. Bongaarts, F.R. van Bure, K. Delcour, J.M. Wigman, Stud. Surf. Sci. Catal. 31 (1987) 83.

[16] P.J. van den Brink, A. Schloten, A. van Wageningen, M.D.A. Lamers, A.J. van Dillen, J.W. Geus, Stud. Surf. Sci. Catal. 63 (1991) 527.
[17] D.J. Lensveld, J.G. Mesu, A.J. van Dillen, K.P. de Jong, Micropor. Mesopor. Mater. 44–45 (2001) 401.
[18] D. Eliche-Quesada, J. Mérida-Robles, P. Maireles-Torres, E. Rodríguez-Castellón, A. Jiménez-López, Langmuir 19 (2003) 4985.
[19] C.T. Kresge, M.H. Leonowicz, W.J. Roth, J.C. Vartuli, J.S. Beck, Nature 359 (1992) 710.
[20] J.S. Beck, J.C. Vartuli, W.J. Roth, M.E. Leonowicz, C.T. Kresge, K.D. Schmitt, C.T.W. Chu, D.H. Olson, E.W. Sheppard, S.B. McCullen, J.B. Higgins, J.L. Schlenker, J. Am. Chem. Soc. 114 (1992) 10834.
[21] A. Corma, Chem. Rev. 97 (1997) 2373.
[22] U. Ciesla, F. Schüth, Micropor. Mesopor. Mater. 27 (1999) 131.
[23] D. Trong On, D. Desplantier-Giscard, C. Danumah, S. Kaliaguine, Appl. Catal. A 253 (2003) 545.
[24] P. Braos-García, P. Maireles-Torres, E. Rodríguez-Castellón, A. Jiménez-López, J. Mol. Catal. A 193 (2003) 185.
[25] D.J. Jones, J. Jiménez-Jiménez, A. Jiménez-López, P. Maireles-Torres, P. Olivera-Pastor, E. Rodríguez-Castellón, J. Rozière, Chem. Commun. (1997) 341.
[26] E. Rodríguez-Castellón, A. Jiménez-López, P. Maireles-Torres, D.J. Jones, J. Rozière, M. Trombetta, G. Busca, M. Lenarda, L. Storaro, J. Solid State Chem. 175 (2003) 159.
[27] A.O. Bianchi, M. Campanati, P. Maireles-Torres, E. Rodríguez-Castellón, A. Jiménez-López, A. Vaccari, Appl. Catal. A 220 (2001) 105.
[28] N.T. Dung, D. Tichit, B.H. Chiche, B. Coq, Appl. Catal. A 169 (1998) 179.
[29] F. Medina-Cabello, D. Tichit, B. Coq, A. Vaccari, N.T. Dung, J. Catal. 167 (1997) 142.
[30] A. Lewandowska, S. Monteverdi, M. Bettahar, M. Ziolek, J. Mol. Catal. A 188 (2002) 85.
[31] K. Hadjiivanov, M. Mihaylov, D. Klissurski, P. Stefanov, N. Abadjieva, E. Vassileva, L. Mintchev, J. Catal. 185 (1999) 314.
[32] G. Busca, Phys. Chem. Chem. Phys. 1 (1999) 723.
[33] M. Trombetta, G. Busca, S. Rossini, V. Piccoli, U. Cornaro, A. Guercio, R. Catani, R.J. Willey, J. Catal. 179 (1998) 581.
[34] A. Streitwieser, C.H. Heathcock, Química Orgánica, McGraw-Hill, New York, 1989, p. 756.
[35] M.J.F.M. Verhaak, A.J. van Dillen, J.W. Geus, J. Catal. 143 (1993) 187.
[36] C.V. Rode, M. Arai, Y. Nishiyama, J. Mol. Catal. A 118 (1997) 229.
[37] M. Arai, Y. Takada, T. Ebina, M. Shirai, Appl. Catal. A 183 (1999) 365.
[38] D. Lin-Vien, N.B. Colthup, W.G. Fateley, J.G. Grasselli, The Handbook of Infrared and Raman Characteristic Frequencies of Organic Molecules, Academic Press, New York, 1991.
[39] K. Hasiguchi, Y. Hamada, M. Tsuboi, Y. Koga, S. Kondo, J. Mol. Spectroscopy 105 (1984) 81.